

GT2011-458),

A NEW APPROACH FOR COMPRESSOR ENDWALL CONTOURING

Alexander Hergt, Robert Meyer, Karsten Liesner, Eberhard Nicke

German Aerospace Center (DLR)
Institute of Propulsion Technology
Linder Hoehe
51147 Cologne, Germany
Email: alexander.hergt@dlr.de

ABSTRACT

Against the background of the high development status of modern axial compressors, a further performance enhancement is linked with the extension of the design space in the development process and the concentration on the essential loss mechanisms in the compressor.

The performance of a compressor cascade is considerably influenced by secondary flow effects in the near end-wall region, since up to 50 percent (for low aspect ratio) of the losses in the bladed channel of a turbomachinery are linked to the endwalls. In this context the application of non-axisymmetric profiled endwalls provides a potential for compressor improvement.

The paper presents the detailed experimental and numerical investigation of controlling the endwall cross flow in a compressor cascade. The general approach is based on a boundary layer fence arrangement, whose application on the compressor endwall works as a non-axisymmetric endwall contour. This non-axisymmetric endwall modification constrains the interaction of the endwall cross flow with the suction side boundary layer, thus the onset of the corner separation is delayed and a significant loss reduction of 8 percent is achieved. The experiments were carried out in a linear compressor cascade at the high-speed cascade wind tunnel of the DLR in Berlin at peak efficiency (design point) and off-design of the cascade at Mach number $M = 0.67$. Furthermore, high fidelity 3D-RANS flow simulations were performed in order to analyze the complex blade and endwall boundary layer interaction. The combined consideration of experimental and numerical flow pattern allows a detailed interpretation and description of the resulting flow phenomena.

NOMENCLATURE

Latin

b	width
c	profile chord length
h	blade span, fence height
deHaller	deHaller number = v_2/v_1
i	incidence angle = $\beta_1 - \beta_{1,Design}$
l	length
M	Mach number
p	pressure
Re	Reynolds number based on chord length
t	pitch
v	velocity
x, y, z	cartesian coordinates

Greek

β	flow angle with respect to cascade front
ϵ	cascade deflection angle = $\beta_1 - \beta_2$
ω	total pressure loss coefficient = $(p_{t,1} - p_{t,2}) / p_{t,1} - p_1$
Ω	static pressure ratio = $p_2 - p_1 / p_{t,1} - p_1$

Subscripts

1	inlet plane
2	exit plane
ax	axial
is	isentropic
t	total, stagnation value

Abbreviations

ADP	aerodynamic design point
AVDR	axial velocity density ratio
EF	endwall-fence
MP1	measurement plane 1 (inlet)
MP2	measurement plane 2 (exit)

INTRODUCTION

The Secondary flow phenomena in the endwall region of compressor blade cascades are well known and described in detail since the early 1950's [1], [2], [3], [4], [3], [5], [6]. These secondary flow effects, in particular the interaction of the endwall cross flow with the blade suction side boundary layer and the resulting corner separation are fundamentally limiting factors of compressor performance and efficiency. Hence, a further improvement of compressor efficiency is directly linked with the influencing of the endwall cross flow and prevention of the corner separation.

In this context, the research is nowadays focused on shaping three dimensional blades and non-axisymmetric endwalls. The developed bowed blade design, as described by Weingold et al. [7], [8], Lyes and Ginder [9] as well as Fischer et al. [10] offers an opportunity to reduce endwall losses by uploading the endwall blade corner region. In this process, the smooth passage of the cross flow from the endwall towards the blade suction side is the fundamental effect which influences the cascade flow and prevents the corner separation.

Concerning the development of non-axisymmetric contoured endwalls Dorfner et al. [11], [12], [13] and Hergt et al. [14], [15] [16] have recently shown that the application of these endwall modifications can be very successful in axial compressors in order to influence the endwall cross flow. Their investigated endwall contour works as an aerodynamic separator, preventing the endwall cross flow from interaction with the blade boundary layer. This method of operation is comparable with the application of vortex generators on the endwall, which was investigated by Hergt et al. [17], [6], [18].

Against this background the idea of the present work was to develop a simple non-axisymmetric endwall modification using a boundary layer fence arrangement in order to deflect the endwall cross flow downstream and prevent its interaction with the blade suction side boundary layer. Thereby the losses which are caused by the corner separation shall be reduced. In a study done by Rockenbach und Brent [19] the application of a boundary layer fence on the compressor endwall above the blade suction side was investigated. In this case, the minimum losses were shifted to higher incidence angles and the deflection close to the endwall was reduced. Furthermore, this investigation shows that the flow control effectiveness of boundary layer fences depends on their number of items and arrangement on the endwall. Furthermore, in previous studies, done by Meyer et al. [20] and Liesner et al. [21], the possibility of loss reduction by boundary layer fences on the cascade endwall was shown.

For this reason, the present investigation was started with a parametric study in order to detect the dependency of cascade losses on the number and arrangement of boundary layer fences (endwall fences). Thereafter, the

fence configuration with the maximum cascade loss reduction was numerically and experimentally investigated in detail. The outcome of this, provides a better understanding of the correlation between the resulting flow structures in the cascade endwall region and the achieved performance enhancement. Finally, the results of the study give an indication on how the compressor endwall could be shaped to unload the cascade.

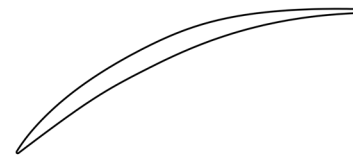
EXPERIMENTAL AND NUMERICAL SETUP

Baseline Linear Cascade The baseline configuration is a high-speed compressor cascade consisting of 5 blades with a NACA-65 K48 profile. The blade profile as well as the general design parameters of the cascade and the test conditions at the aerodynamic design point (ADP) are shown in Table 1.

The cascade blades have an aspect ratio of 1 which was selected in order to emphasize secondary flow effects. Furthermore, this value is typical for rear stages of high pressure compressors. In addition, the cascade enables tests at realistic flow conditions, e.g. Mach number, thus transferability to real turbomachines is possible to a certain extent.

The cascade measurements were carried out at cascade design Mach number of 0.67. Based on the design inflow angle ($\beta_1 = 132$ deg.) measurements at positive as well as negative incidence angles ($i = 2, 4, 6$ deg. and $-2, -4$ deg.) were performed in order to analyze the cascade behavior over the operation range.

Table 1: NACA-65 K48 profile (top), cascade design parameters and test conditions at ADP



Inlet Mach number	M_1	= 0.67
Inlet flow angle	β_1	= 132°
Stagger angle	β_{st}	= 112.5°
Blade chord	c	= 40 mm
Blade span	h	= 40 mm
Blade aspect ratio	h/c	= 1
Pitch to chord ratio	t/c	= 0.55
Incoming endwall boundary layer thickness absolute	δ	= 4 mm

Endwall Fence Cascade For a variable endwall fence (EF) arrangement both cascade endwalls were constructed with 8 slots as shown in Fig. 1. The pitchwise distance between the slots amounts to $y/t = 0.082$ and the axial length l ranges from $x/c_{ax} = 0.5$ to $x/c_{ax} = 1$ (trailing edge position). The used endwall fences consist of sheet metal plates with 0.1 mm thickness and are inserted in the slots, thus their height h is variable by the insertion depth. In addition, the leading edges of the fences are swept with an angle of 45 deg. The parameters for the endwall fence arrangement are defined in Fig. 2.

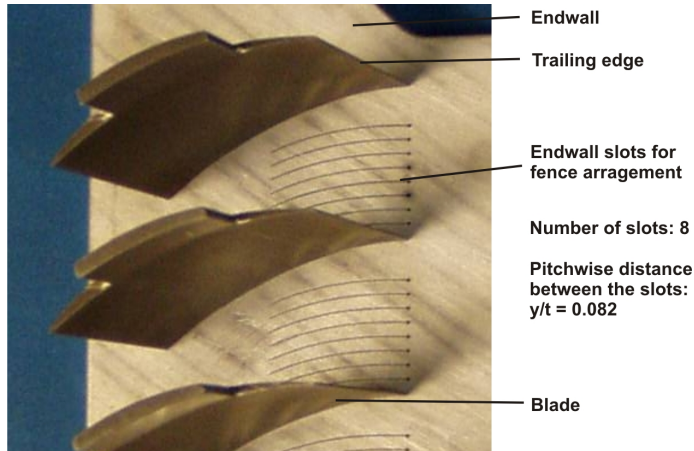


Figure 1: Slot configuration on the cascade endwall

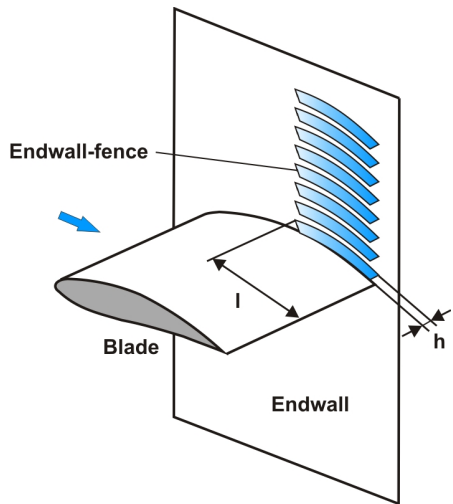


Figure 2: Basic endwall fence parameters

Test Facility and Measurement Techniques The experiments were carried out at the high-speed cascade

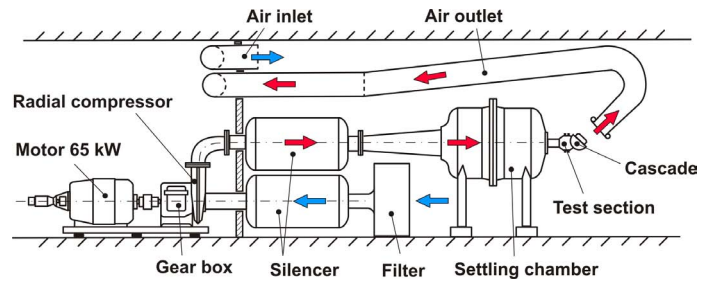


Figure 3: High-speed cascade wind tunnel

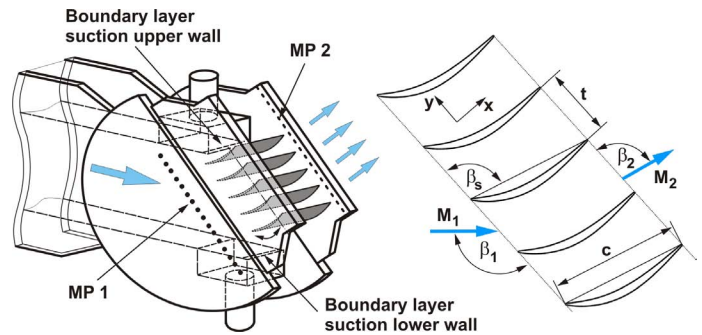


Figure 4: Test section and cascade parameters

wind tunnel of DLR (Institute of Propulsion Technology) in Berlin. The wind tunnel, as shown in Fig. 3, has a rectangular cross section of 40 mm width and 90 mm height at the exit nozzle (contraction ratio 1:218) of the settling chamber. Thus, flow conditions of $M_1 = 0.7$ with $Re = 0.6 \times 10^6$ can be obtained [22]. The test section of the wind tunnel with the attached cascade and the definition of the cascade parameters is shown in Fig. 4.

For the tests the blade chord Reynolds number was around 0.56×10^6 at $M_1 = 0.66$. The inflow Mach number was determined at measurement plane 1 (MP1) by measuring the static inlet pressure at this plane as well as the total pressure and total temperature within the settling chamber. Furthermore, the incoming endwall boundary layer thickness at MP1 was also determined and amounts to 4 mm, which corresponds to about 20 percent of half span.

The total pressure distribution in the wake is measured with a wake rake placed 40 percent of chord length c behind the trailing edge of the cascade blades consisting of 26 pitot probes, which are equally distributed from endwall to endwall. In addition, the outflow angle is measured at four blade height positions with a second rake consisting of four Conrad probes, which are located at 0.087, 0.2, 0.325 and 0.45 z/h . Furthermore, the static pressure at midspan was measured with the second rake and experimental flow visualization by means of oil streak patterns was performed in order to obtain a detailed description and interpretation of the flow phenomena in the endwall region. A detailed description of the measurement technique, data acquisition and analysis of the wake measure-

ment at the high-speed cascade wind tunnel of DLR (Institute of Propulsion Technology) is given by Liesner and Meyer [23]

The estimation of the experimental accuracy yields a uncertainty of ± 1.2 percent of the total pressure loss coefficient and ± 0.5 deg. of the outflow angle.

Numerical Approach For comparison with the experimental results and in order to analyze the flow phenomena in the endwall region in detail, steady numerical simulations with DLR's 3D-RANS flow solver TRACE, including a $k-\omega$ turbulence model, were carried out at the aerodynamic design point of the datum cascade and the EF cascade at the measured inflow conditions ($M_1 = 0.67$, $\beta_1 = 132$ deg.). Convergence massflow as well as the global mean residue, which had to be less than 1×10^{-6} , were considered. For both cascades a fine multi-block grid with a OCH topology was used in order to sufficiently resolve the blade and endwall boundary layer. The grid of the datum cascade consists of nearly 1.3 million nodes. For the simulation with the EF cascade a grid of nearly 4.5 million nodes was constructed as shown in Fig. 5, where the fences were shaped by small H-blocks with a thickness of one cell. The panels of these blocks were defined as viscous walls.

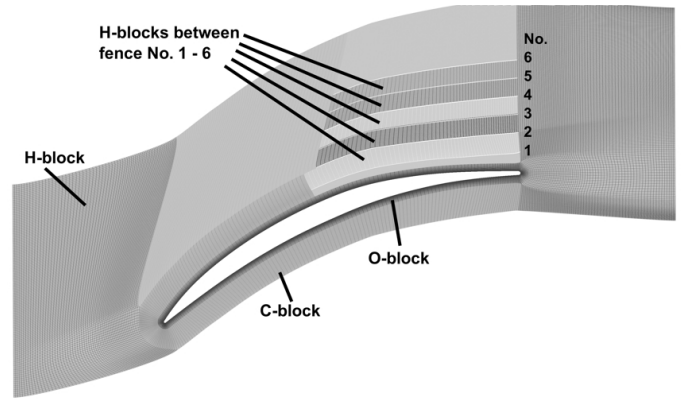


Figure 5: Grid of the EF cascade

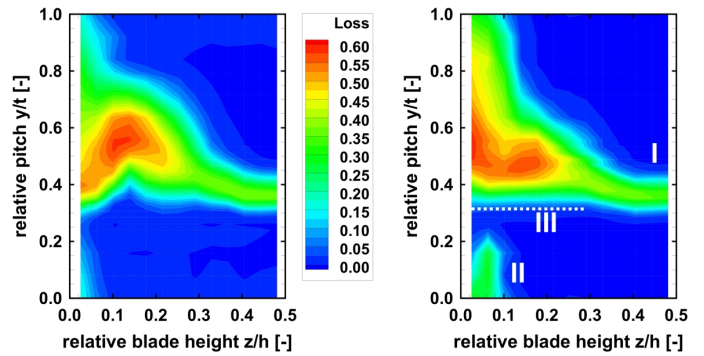


Figure 6: Measured total pressure loss distribution at MP2 for the datum cascade (left) and the EF cascade with 8 fences of height $h = 4$ mm (right)

RESULTS AND DISCUSSION

Approach of endwall fence arrangement In the first step of the study the correlation between the fence arrangement and the cascade losses is identified by a variation of the fence number and height at ADP. In Tab. 2 the different configurations of the endwall fences and the resulting cascade losses ω are listed. These results show that for the EF configurations with 8 fences (max. number) of equal height h the impact on cascade losses are marginal.

Nevertheless, the loss distribution is significantly influenced as exemplified in Fig. 6. This figure shows the

Table 2: Parameter and measurement results of the endwall fence arrangement study at ADP

No. of fence	height h [mm]	Loss ω [-]
0 (datum)	0	0.097
1 - 8	0.4	0.096
1 - 8	0.7	0.095
1 - 8	1.0	0.096
1 - 8	2.0	0.096
1 - 8	3.0	0.095
1 - 8	4.0	0.096
1 - 4	4.0/3.0/2.0/1.0	0.094
1 - 6	4.0/3.0/2.0/1.0/0.7/0.4	0.089

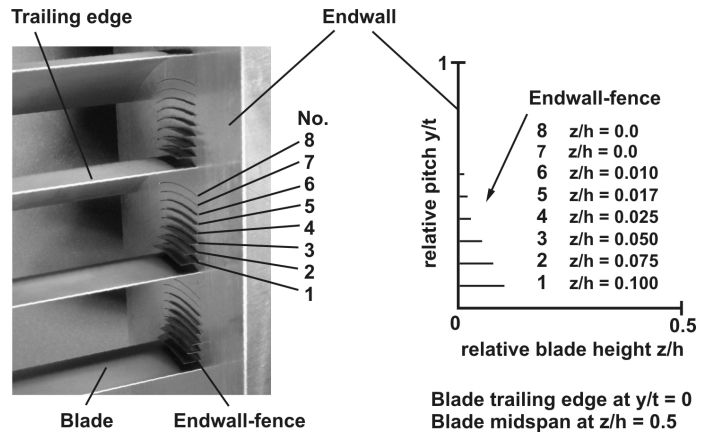


Figure 7: Optimal endwall fence arrangement

measured total pressure loss distribution for the datum cascade and EF cascade with 8 fences of 4 mm height. Three basic effects can be deduced from the comparison of these results. The losses in the midspan region are reduced (marked with I) and close to the endwall at relative pitch positions from $y/t = 0$ to 0.2 (marked with II) and 0.8 to 1.0

the losses are increased. Furthermore, the loss wake is at relative pitch $y/t = 0.4$ from the endwall to relative span position $z/h = 0.3$ in a line, which leads to a more uniform spanwise outflow angle distribution. The outcome of this is, in the case of a multi-stage compressor, a more uniform inflow condition to the next stage in the endwall region, which is an important design criterion.

From these results the design of an optimal fence arrangement can be extracted. The fence of height $h = 4$ mm close to the blade suction side effectively influences the loss and outflow angle distribution. The fence heights h have to be reduced with the increase of relative pitch position, towards the blade pressure side of the adjacent blade, otherwise they massively block the endwall cross flow and produce high additional losses. Hence, an optimal fence arrangement has staged fence height h as shown in Fig. 7. A significant cascade loss reduction of 9 percent was achieved by this EF configuration. Subse-

quently, this EF cascade is investigated in detail in order to understand the effect on the endwall boundary layer behaviour, loss characteristics and cascade performance.

Endwall boundary layer behaviour Figure 8 and 9 show the oil-flow visualization and the numerical streak lines on the endwall of the datum and EF cascade. For the datum cascade the typical endwall cross flow is visible as well as the corner separation in the rear part of the blade. This separation is represented by the reverse flow in the numerical streak lines and the congeries of the white oil in the experimental flow visualization.

The topology of the endwall flow is significantly changed for the EF cascade, since the cross flow is blocked and downstream deflected by the fences. Between the fences number 1 to 5 a conducted downstream flow is vis-

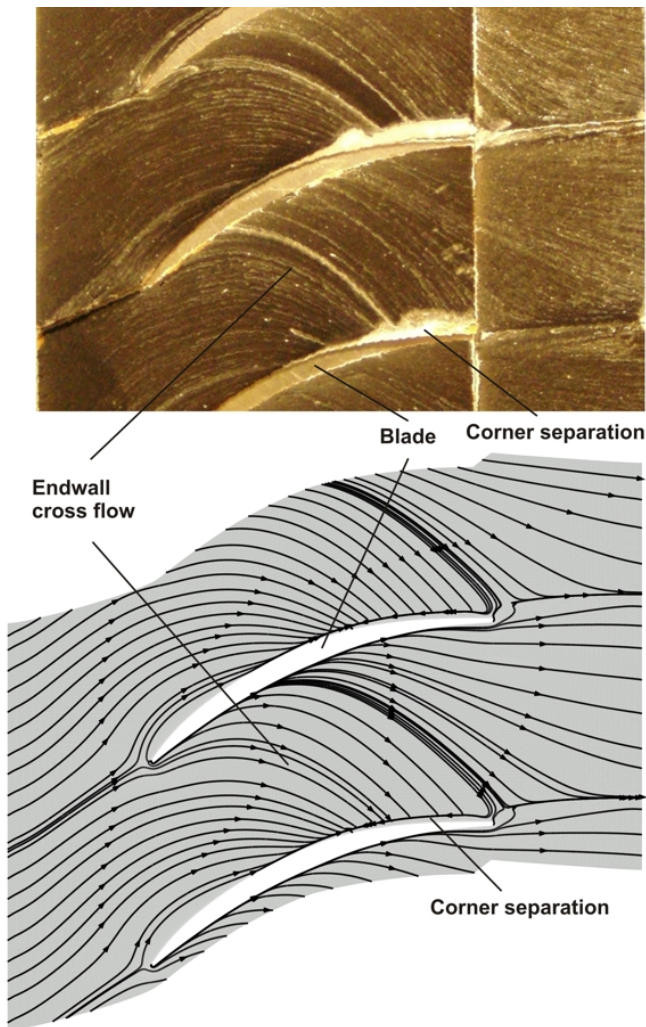


Figure 8: Oil-flow visualization (top) and numerical streak lines (bottom) on the endwall of the datum cascade at ADP

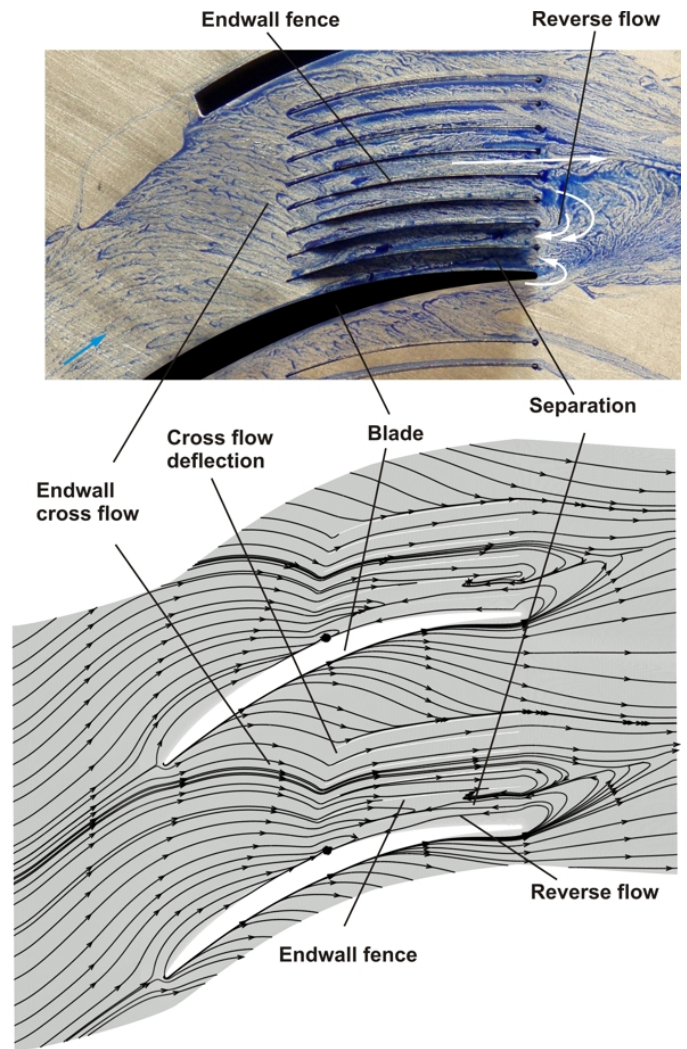


Figure 9: Oil-flow visualization (top) and numerical streak lines (bottom) on the endwall of the optimal EF cascade at ADP

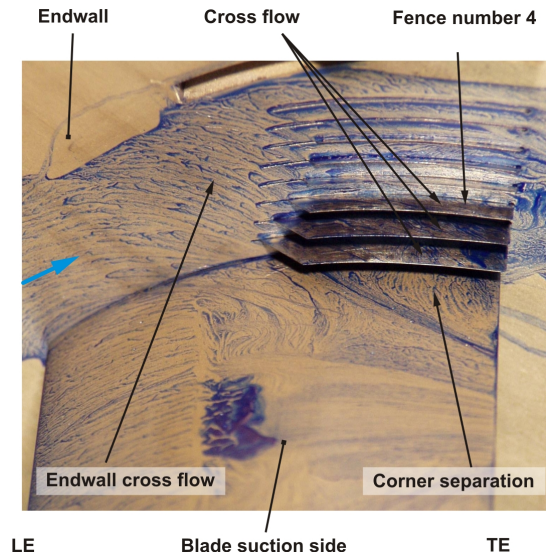
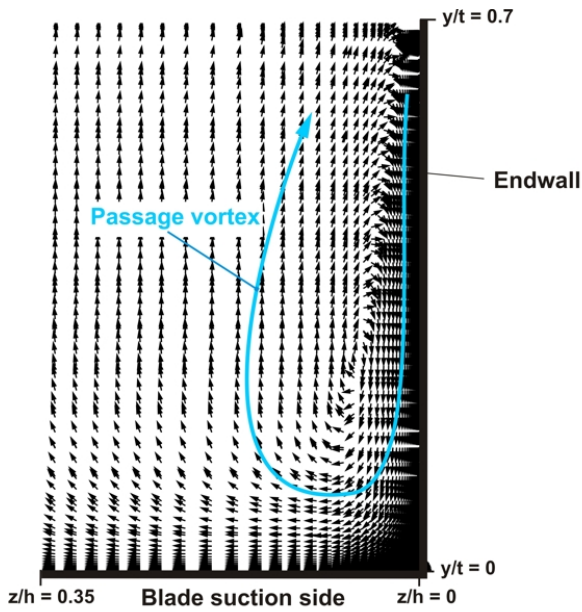


Figure 11: Oil-flow visualization on blade suction side and endwall of the EF cascade at ADP

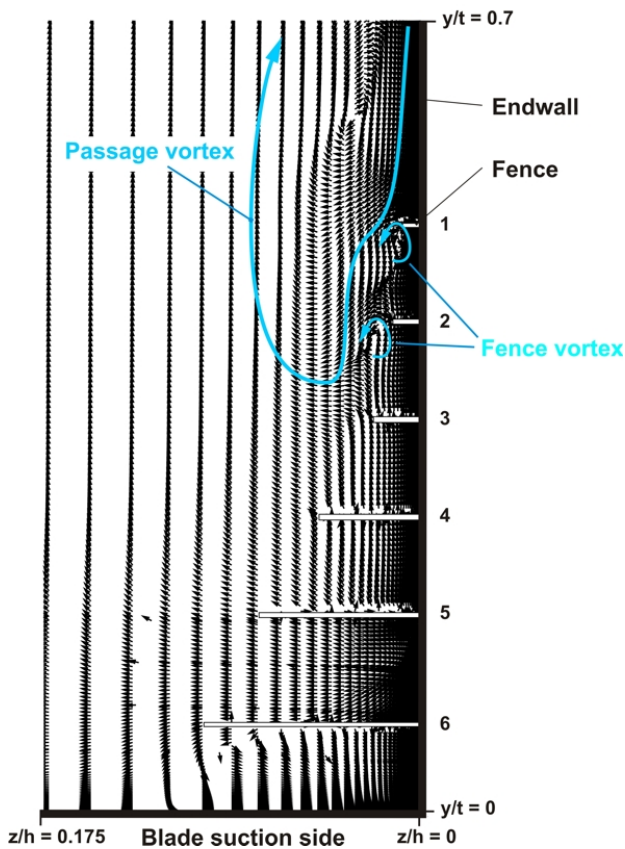


Figure 10: Simulated secondary flow vectors in a x -plane at $x/c_{ax} = 0.95$ of the datum (top) and EF cascade (bottom) at ADP, view direction is upstream

ible. Furthermore, between the blade and fence number 6 as well as between fences number 6 and 5 a reverse flow with separation exists. These reverse flows are extended

behind the trailing edge of the cascade as shown in Fig. 9. In addition to the flow visualization on the endwall the secondary flow vectors in the x -plane at $x/c_{ax} = 0.95$ shown in Fig. 10 clarify the impact of the endwall fences on the passage vortex, whose existence results from the endwall cross flow. In this figure the separation of the passage vortex from the endwall due to the staged endwall fence arrangement is observable. At fences number 1 and 2 vortices appear (fence vortex) with rotational sense in opposite direction to the passage vortex. These vortices results from the incoming cross flow to the fences on the endwall.

Furthermore, Fig. 10 (bottom) shows that the pitch-wise extension of the passage vortex is reduced and its interaction with the blade suction side boundary layer is prevented, which results from the effect of fences number 1 and 2. The arrangement of these fences is the reason for the significant loss reduction, because the achievable loss reduction is much lesser without these both fences as shown by the results in Tab. 2 (second last line). In the case of fence arrangement as described in the second last line in Tab. 2 the endwall cross flow is not moved away from the endwall but massively blocked by the fence number 3 of 1 mm height. For this reason additional losses occur.

The cross component of the flow decreases with the increasing distance from the endwall, thus the fences number 4, 5 and 6 operate as blade profiles. Figure 11 shows the oil flow visualisation on the endwall, the blade suction side and the endwall fences. In this figure the reverse and cross flow on the uppers side of the fences number 4, 5, 6 are observable. This behaviour is comparable with the development of the original corner separation and result from the pressure rise in the cascade.

Nevertheless, the corner separation has not dissa-

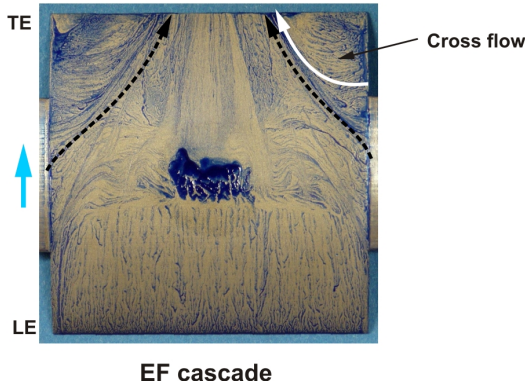
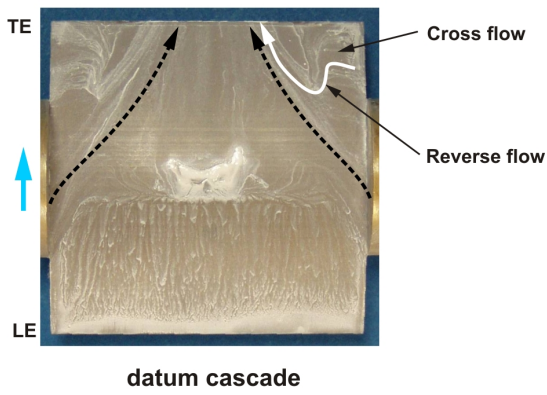


Figure 12: Oil-flow visualization on blade suction side of the datum (top) and EF cascade (bottom) at ADP

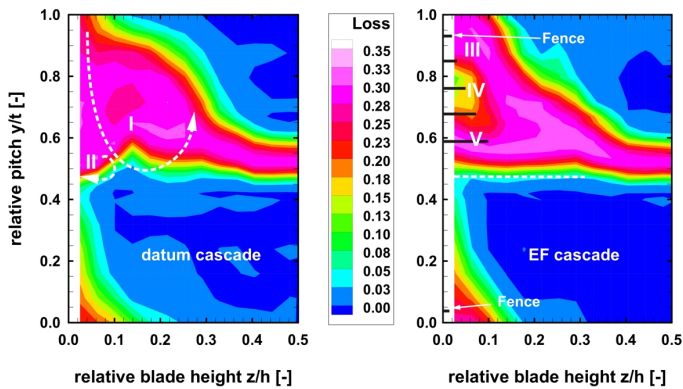


Figure 13: Measured mass-flow averaged total pressure loss distribution of the datum (left) and EF cascade (right) at MP2, ADP

peared as shown in the oil flow visualization in Fig 12, but the topology of the separation is significantly changed. The extension of the separated area on the blade suction side is reduced and the typical reverse flow does not occur, which leads to a reduction of the total pressure loss.

This described behaviour is reflected by the total pressure loss distribution as shown in Fig. 13, where the posi-

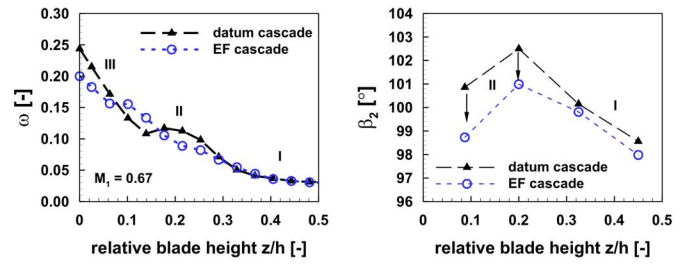


Figure 14: Measured spanwise distribution of pitchwise averaged total pressure loss (left) and deflection difference (right) at MP2, ADP and $i = +4$ deg.

tions of the fences are marked for the EF cascade. In the left diagram the loss distribution behind the datum cascade with the typical shape resulting from the secondary flow in the cascade is diagrammed. The rotational movement of the passage vortex is represented by the arrow marked with I and the resulting corner vortex, which rotates in the opposite direction, is represented by the arrow number II. In comparison with the EF cascade it is noticeable that the typical shape of the loss distribution is changed. The loss wake is at relative pitch $y/t = 0.5$ from the endwall to relative span position $z/h = 0.3$ in a line. This indicates that the original development of the passage vortex (I) and the resulting corner vortex (II) is suppressed by the endwall fences, which leads to a more uniform spanwise outflow angle distribution as shown in Fig. 14. The right diagram shows the spanwise distribution of the pitchwise averaged outflow angle of the datum and the EF cascade at the ADP. For this operation point the outflow angle in the midspan region ($z/h = 0.3$ to 0.5 , marked with I) is slightly influenced. In the spanwise region towards the endwall (marked with II) the outflow angle is decreased, which means an increase of deflection and a more uniform outflow angle distribution.

Concerning the total pressure loss distribution in Fig. 13 it has further to be mentioned that the losses at midspan region from z/h 0.3 to midspan (marked with I in Fig. 14) are not influenced by the endwall fences. This behaviour is also reflected by the loss curves in the left diagram of Fig. 14, which shows the spanwise distribution of the pitchwise averaged total pressure loss of the datum and the EF cascade at the ADP. In addition to that, the losses in the spanwise region between $z/h = 0.2$ to 0.3 (marked with II in Fig. 14) are reduced.

The most significant change in the loss distribution in Fig. 13 and 14 is observable in the spanwise region between the endwall and $z/h = 0.2$ (marked with III in Fig. 14). The loss region is extended there in pitchwise direction (Fig. 13) but due to the loss region marked with IV, where the loss intensity is decreased, the pitchwise averaged losses are also reduced. The high loss region, marked with III, results from the described fence vortices (fences

number 1 and 2) and the high loss region, marked with V, results from the separation between the blade suction side and fences number 4, 5, 6 as already shown in Fig. 12 and 10.

The following step of the current study includes the investigation of the loss characteristics and performance of the EF cascade over their operation range.

Loss characteristics and cascade performance

Figure 15 shows the loss curve of the datum and the EF cascade. In this figure it is noticeable that the characteristic of the loss is significantly changed by the end-wall fences. In addition to the loss reduction at the ADP, the losses at negative incidence angle are also significantly decreased. At positive incidence angles of 4 deg. and 6 deg. the losses are increased, thus the curve seems to be turned. In order to assess this loss behaviour, the performance data in terms of deflection, AVDR, deHaller number and static pressure ratio at midspan have to be considered as shown in Figure 16. In this figure the measured curves at midspan of this performance data are diagrammed and it is visible, that the AVDR at negative incidence angle is only marginally influenced, whereas at positive incidence angle it is increased. This increase of the AVDR indicates that the blockade in the cascade endwall region due to the endwall fences also increases. For this reason the loss increase can be traced back to an increase of additional loss production by the endwall fences.

The increase of AVDR at positive incidence angles leads to a reduction of blade loading at midspan, which is reflected by the decrease of the 1-deHaller number as well as the decrease of the static pressure rise. This behavior corresponds with the influence of the AVDR on deflection and static pressure rise described by Schreiber and Starcken [24].

At negative incidence angles an influence of the end-wall fence arrangement on the cascade deflection is detectable. In spite of unaffected AVDR and pressure rise the deflection is increased. This considerably results from the

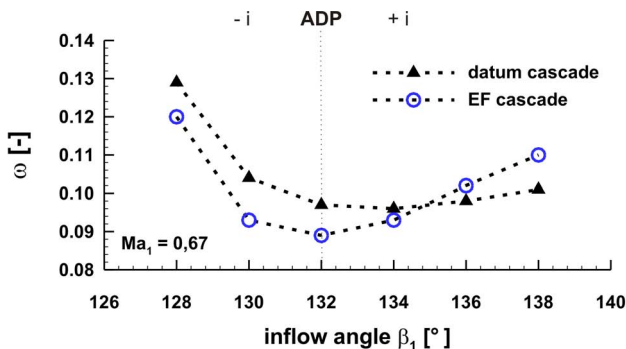


Figure 15: Mass-flow averaged total pressure loss coefficient ω of the datum and EF cascade

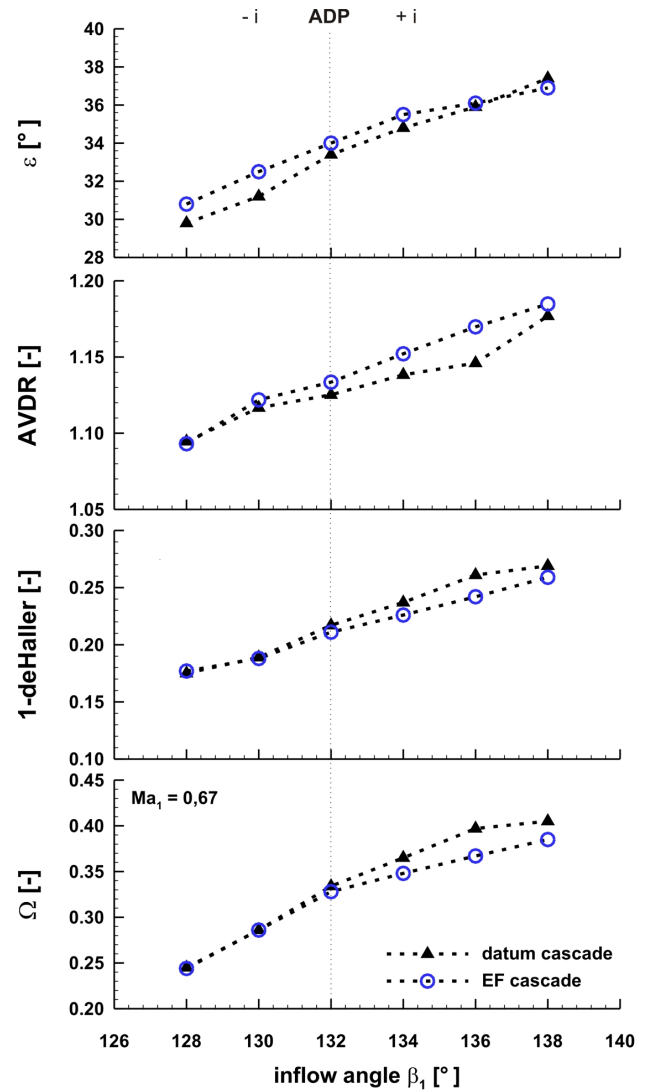


Figure 16: Deflection ϵ , AVDR, 1-deHaller and static pressure ratio Ω at midspan of the datum and EF cascade

significant loss reduction at these operation points.

CONCLUSION AND OUTLOOK

In summary, it can be stated that the investigated end-wall modification by a boundary layer fence arrangement shows a significant influence on the endwall cross flow and thereby on the cascade loss distribution. The endwall cross flow was blocked and deflected downstream, thereby preventing the interaction of the cross flow with the suction side blade boundary layer. This leads to a reduction of the corner separation and a decrease of cascade losses at the ADP of about 9 percent. Furthermore, a more uniform spanwise outflow angle distribution was achieved.

These results of the investigation are considerably caused by the staged arrangement of the fences, hence the cross flow was moved away from the endwall and its ex-

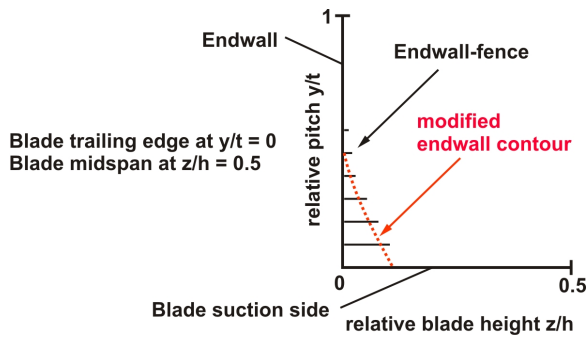


Figure 17: Modified endwall contour and fence arrangement

tension to the blade suction side was bounded. Moreover, the fences with large heights produce additional losses due to existing reverse flow between the fences as well as on the endwall behind the fences. In future investigations the endwall contour between the fences could be modified as shown in Fig. 17 in order to minimize the fence surface, avoid such reverse flow and achieve further loss reduction.

Furthermore, from the results of this study a fundamental design criterion for endwall modifications can be deduced. The aim of endwall modifications should be focused on the smooth deflection and guiding of the endwall cross flow in order to delay or prevent its interaction with the blade boundary layer.

Generally, the outcome of this study shows that endwall modification based on non-axisymmetric endwall contouring and the use of flow control devices like boundary layer fences offer the possibility to reduce secondary flow losses and enhance the performance of compressor cascades. Further studies should be focused on the improvement of the effectiveness of non-axisymmetric endwall modifications and their inclusion into the compressor design process.

REFERENCES

- [1] Herzig, H. Z., Hansen, A. G., and Costello, G. R., 1953. Visualization of Secondary Flow in Compressor Cascades. Technical Report 1163, NACA.
- [2] Horlock, J. H., Luis, J. F., Percival, P. M. E., and Lakshminarayana, B., 1966. "Wall Stall in Compressor Cascades". *Journal of Basic Engineering, ASME*, September, pp. 637–648.
- [3] Schlichting, H., and Das, A., 1966. "Recent Research on Cascade-Flow Problems". *Journal of Basic Engineering, ASME*, March, pp. 221–228.
- [4] Horlock, J. H., and Lakshminarayana, B., 1973. "Secondary Flow: Theory, Experiment, and Application in Turbomachinery Aerodynamics". *Annual Review of Fluid Mechanics*, 5, pp. 247–280.
- [5] Gbadebo, S. A., Cumpsty, N. A., and Hynes, T. P., 2005. "Three-Dimensional Separations in Axial Com-

- pressors". *Journal of Turbomachinery, ASME*, 127(2), April, pp. 331–339.
- [6] Hergt, A., Meyer, R., and Engel, K., 2010. "Effects of Vortex Generator Application on the Performance of a Compressor Cascade". No. GT2010-22464 in ASME Turbo Expo.
- [7] Weingold, H., Neubert, R., Behlke, R., and Potter, G., 1995. "Reduction of Compressor Endwall Losses through the Use of Bowed Stators". No. 95-GT-380 in ASME Turbo Expo.
- [8] Weingold, H., Neubert, R., Behlke, R., and Potter, G., 1997. "Bowed Stators an Example of CFD Applied to Improve Multistage Compressor Cascade". *Journal of Turbomachinery, ASME*, 119(2), April, pp. 161–166.
- [9] Lyes, P. A., and Ginder, R. B., 1999. "Compressor Test of Bowed and Swept Blades". No. ISABE 99-7048 in ISABE, ISABE and AIAA.
- [10] Fischer, A., Riess, W., and Seume, J. R., 2004. "Performance of Strongly Bowed Stators in a Four-Stage High-Speed Compressor". *ASME Journal of Turbomachinery*, 126(3), July, pp. 333–338.
- [11] Dorfner, C., Nicke, E., and Voss, C., 2007. "Axis-Asymmetric Profiled Endwall Design by using Multi-objective Optimisation Linked with 3D RANS-Flow-Simulations". No. GT2007-27268 in ASME Turbo Expo.
- [12] Dorfner, C., 2009. "Entwicklung eines Verfahrens zur Konstruktion nicht-rotationssymmetrischer Seitenwandkonturen in axialen Verdichtern". DLR Forschungsbericht, Ruhr-Universität Bochum.
- [13] Dorfner, C., Hergt, A., Nicke, E., and Mönig, R., 2011. "Advanced Non-Axisymmetric Endwall Contouring for Axial Compressors by Generating an Aerodynamic Separator Part I: Principal Cascade Design and Compressor Application". *ASME Journal of Turbomachinery*, 133, April, pp. 021026–1 – 021026–6.
- [14] Hergt, A., Dorfner, C., Steinert, W., Nicke, E., and Schreiber, H. A., 2011. "Advanced Non-Axisymmetric Endwall Contouring for Axial Compressors by Generating an Aerodynamic Separator Part II: Experimental and Numerical Cascade Investigation". *ASME Journal of Turbomachinery*, 133, April, pp. 021027–1 – 021027–8.
- [15] Hergt, A., Kinner, J., Steinert, W., Dorfner, C., and Nicke, E., 2011. "Detailed Flow Analysis of a Compressor Cascade with a Non-Axisymmetric Endwall Contour". No. 95 in 9th European Turbomachinery Conference.
- [16] Hergt, A., Steinert, W., Dorfner, C., Nicke, E., and Berversdorff, M., 2009. "Experimental and Numerical Investigation of a Novel Compressor Endwall Design". 7th World Conference on Experimental Heat Transfer, Fluid Mechanics and Thermodynamics.
- [17] Hergt, A., Meyer, R., Müller, M., and Engel, K., 2008. "Loss Reduction in Compressor Cascades by Means of Passive Flow Control". No. GT2008-50357 in ASME

- Turbo Expo.
- [18] Hergt, A., 2011. "Über grenzschichtbeeinflussende Maßnahmen in den Randzonen von Verdichtergittern (in press)". PhD thesis, Technische Universität Berlin.
 - [19] Rockenbach, R. W., and Brent, J. A., 1971. Single Stage Experimental Evaluation of Compressor Blading with Slots and Wall Flow Fences. Technical Report NASA CR-72635, NASA.
 - [20] Meyer, R., and Hage, W., 2008. "Secondary flow control on axial compressor blades by passive and active methods". No. AIAA-2008-4320 in 4th AIAA Flow Control Conference.
 - [21] Liesner, K., Meyer, R., Hage, W., and Paschereit, C. O., 2008. "Off-Design Study of Secondary Flow Control Using Contoured Plates on High-Speed Compressor Cascade Walls". Int. Conf. on Jets, Wakes and Separated Flows, ICJWSF, Berlin Institute of Technology.
 - [22] Meyer, R., Bechert, D. W., and Hage, W., 2003. "Secondary Flow Control on Compressor Blades to Improve the Performance of Axial Turbomachines". 5th European Turbomachinery Conference.
 - [23] Liesner, K., and Meyer, R., 2008. "Experimental Setup for Detailed Secondary Flow Investigation by Two-Dimensional Measurement of Total Pressure Loss Coefficients in Compressor Cascades". XIX Biannual Symposium on Measuring Techniques in Turbomachinery Transonic and Supersonic Flow in Cascades and Turbomachines, VKI.
 - [24] Schreiber, H. A., and Starke, H., 1981. "On the Definition of the Axial Velocity Density Ratio in Theoretical and Experimental Cascade Investigation". Symposium on Measuring Techniques in Transonic and Supersonic Flow in Cascades and Turbomachines.